

Developed empirical model for simulation of time-varying frequency in earthquake ground motion

Ruifang Yu^{1a}, Meiqiao Yuan² and Yanxiang Yu^{*1}

¹*Institute of Geophysics, China Earthquake Administration, Mingzu Daxue South Road No. 5, Haidian District, Beijing, 100081, China*

²*Huaian Guangan Seismic Safety Evaluation Technology Co. Ltd., Huaihai Road 254, Qinghe District, Huai'an, Jiangsu, 223001, China*

(Received July 25, 2014, Revised October 13, 2014, Accepted November 6, 2014)

Abstract. This research aims to develop an empirical model for simulation of time-varying frequency in earthquake ground motion so as to be used easily in engineering applications. Briefly, 10545 recordings of the Next Generation Attenuation (NGA) global database of accelerograms from shallow crustal earthquakes are selected and binned by magnitude, distance and site condition. Then the wavelet spectrum of each acceleration record is calculated by using one-dimensional continuous wavelet transform, and the frequencies corresponding to the maximum values of the wavelet spectrum at a series of sampling time, named predominant frequencies, are extracted to analyze the variation of frequency content of seismic ground motions in time. And the time-variation of the predominant frequencies of 178 magnitude-distance-site bins for different directions are obtained by calculating the mean square root of predominant frequencies within a bin. The exponential trigonometric function is then used to fit the data, which describes the predominant frequency of ground-motion as a function of time with model parameters given in tables for different magnitude, distance, site conditions and direction. Finally, a practical frequency-dependent amplitude envelope function is developed based on the time-varying frequency derived in this paper, which has clear statistical parameters and can emphasize the effect of low-frequency components on later seismic action. The results illustrate that the time-varying predominant frequency can preferably reflect the non-stationarity of the frequency content in earthquake ground motions and that empirical models given in this paper facilitates the simulation of ground motions.

Keywords: earthquake ground motion; time-varying frequency; non-stationarity of frequency; empirical models; envelope function

1. Introduction

Non-stationarity in earthquake ground motions occurs due to the temporal variations in the amplitude and frequency content. Although the temporal non-stationarity of the amplitude of ground motion can be modeled easily by multiplying a stationary process by a time function, the

*Corresponding author, Professor, E-mail: yuyx@cea-igp.ac.cn

^aPh.D., E-mail: yrfang126@126.com

frequency non-stationarity shown in certain spectral form is generally difficult to establish ideal models. In practice, both non-stationarity of amplitude and frequency are important, particularly in analyzing nonlinear seismic response of structures. Consequently, the growing interests in performance-based earthquake engineering (PBEE) has strengthened the need for realistic characterization of ground motion because the PBEE analysis typically considers the entire spectrum of the structural response, from linear to grossly nonlinear and even collapse (Bozorgnia and Bertero 2004, Yang and Wang 2012, Cakir 2013). And the inelastic, degrading structures tend to have resonant frequencies, which decay with time as the structure responds to strong shaking. This trend may coincide with the variation in time of the predominant frequency of the ground motion, thus enhancing the demand (Papadimitriou 1990). Therefore, it is necessary to introduce a general mathematic model to simulate the actual variation of earthquake ground motion except the uniformly modulated process (Housner and Jennings 1964, Nakayama *et al.* 1994, Zhou and Yu 2008, Nimitaj *et al.* 2013). Along with the improvement of time-frequency analysis techniques available for non-stationary signal analysis, such as the short time Fourier transform (STFT), continuous wavelet transform (CWT), Wigner-Ville distribution and Hilbert-Huang transform (Gabor 1946, Rioul and Vetterli 1991, O'Neill *et al.* 1999), the time-frequency joint spectrum is developed, which can describe the non-stationarity of amplitude and frequency for earthquake ground motion more accurately, and are suitable for simulation of actual seismic recordings (Deodatis and Shinozuka 1988, Yeh and Wen 1990, Conte and Peng 1997, Wang *et al.* 2002, Rezaeian *et al.* 2008, Jin *et al.* 2012). However, since the joint description of the time-frequency model includes many influence factors and is too complex to describe, it is difficult to obtain the model statistical parameters used directly in engineering practice. Therefore, the simplified model describing approximately non-stationarity of frequency in earthquake ground motion needs to be considered.

Any satisfying model should be parsimonious, i.e., has as few parameters as possible, and has a form which facilitates the engineering applications. So the main object of this study is to develop empirical models for simulation of non-stationarity of frequency in earthquake ground motion, which can facilitate the engineering application. For this purpose, 10545 recordings from the Next Generation Attenuation (NGA) global database of accelerograms are selected and divided into 178 groups according to the magnitude, distance, site condition and direction. Then one-dimensional continuous wavelet transform (CWT) is used to calculate the wavelet spectrum of each acceleration record, and the frequencies corresponding to the maximum values of the wavelet spectrum at a series of sampling time, named predominant frequencies, are extracted to analyze the variation of the frequency content in earthquake ground motions. And the variations of the predominant frequencies of 178 magnitude-distance-site bins for horizontal and vertical directions are obtained by calculating the mean square root of predominant frequencies within a bin. The exponential trigonometric function is selected to describe the time-varying frequency and the model parameters are given in tables for different magnitude, distance, site conditions and direction. Finally, a practical frequency-dependent amplitude envelope function, which has clear statistical parameters, is developed based on the time-varying frequency to consider the non-stationarity of frequency content in ground motion, especially emphasize the effect of low-frequency components in later seismic action. This model is later proved to be suitable for the simulation of ground motion to reflect the non-stationarity of earthquake acceleration.

2. Data grouping

Table 1 Data grouping according to magnitude, epicentral distance and site condition

M	R/km	0-20			20-40			40-60			60-80			80-100			>100		
	Site	A	B	C	A	B	C	A	B	C	A	B	C	A	B	C	A	B	C
(<5.5)		85	376	82	47	219	33	33	160	45	18	113	12	31	74	27	12	48	21
[5.5,6.0)		53	255	36	45	219	36	36	233	45	36	140	39	30	75	30	60	189	147
[6.0,6.5)		30	74	9	91	216	34	123	569	128	165	521	171	69	392	114	180	732	384
[6.5,7.0)		49	98	37	72	162	68	45	157	63	39	93	32	53	80	18	36	181	25
(≥7.0)		30	18	--	36	95	18	48	87	51	63	235	27	42	168	30	132	782	225

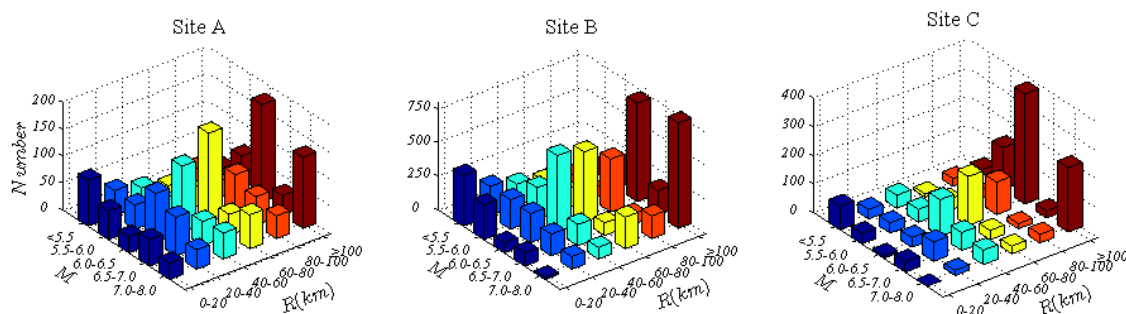


Fig. 1 Distribution of acceleration records according to magnitude, distance and site condition

The strong motion records used here are selected from the NGA database of the United States. The selected 10545 acceleration recordings are all from 173 shallow crustal earthquakes in the intra-plate active tectonic regions worldwide during the years of 1935-2003, ranging in magnitude from 4.27 to 7.9 (Chiou *et al.* 2008). These records are grouped according to three factors, i.e., magnitude (defined as M), epicentral distance (defined as R) and site condition. In this study, the site condition was classified into three categories defined as A, B and C based on the average shear-wave velocity $V_{s,30}$. And the values of $V_{s,30}$ for boundaries of Sites A, B and C are generally equal to 510 m/s, 260 m/s and 150 m/s, respectively, according to the relative research (Lü and Zhao 2007). The authors take every 20 km as interval to divide epicentral distance into six ranges, i.e., [0-20) km, [20-40) km, [40-60) km, [60-80) km, [80-100) km, and (>100) km, and took 0.5 as interval to divide magnitude into five ranges, i.e., (<5.5), [5.5-6.0), [6.0-6.5), [6.5-7.0) and (≥7.0). So acceleration recordings are divided into 90 magnitude-distance-site bins, as is shown in Table 1, in which every group includes two horizontal components and a vertical component, and the symbol "--" indicates no recordings included. The data distribution map, as is shown in Fig. 1, is plotted to exhibit the distribution of the acceleration records.

3. Data processing

3.1 Modification of start point of recordings

Firstly, the start points of acceleration records were modified to decrease the degree of discreteness of data in statistical analysis. Then the time of P-wave first arrival was selected as the

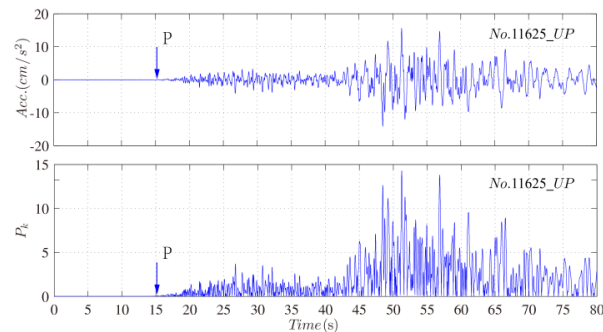


Fig. 2 The identification of P-wave first arrival of acceleration record

start point of acceleration records to both eliminate the effect of random noise and make the frequency at start time having uniform definition. P-wave identification is based on the amplitude variation of recordings, in which characteristic parameters is defined as

$$P_k = \left| \bar{X}_{pk} \right| \quad (1)$$

where \bar{X}_{pk} is the mean value of amplitude in the given time window Δt ($\Delta t = 0.5s$).

The example of identification process of an acceleration time series is shown in Fig. 2. The first jump-point in curve of characteristic parameters P_k is the time of P-wave first arrival, as is shown point “P” in Fig. 2. Every recording is modified by removing the section before the initial P-wave’s arrival.

3.2 Duration of earthquake ground motion

The non-stationarity of frequency content in earthquake ground motion emphasizes the variation along with the time. However, the duration of acceleration records in a magnitude-distance-site bin is different because the duration is usually influenced by magnitude, distance and site condition. Therefore it is necessary to uniform the duration of recordings in a magnitude-distance-site bin for obtaining the statistical characteristic of several acceleration records in a given group during calculating the mean square root of recording parameters in the each bin. The duration of acceleration record can be defined as $t = t_1 + t_s + t_c$, as is shown in Fig. 3, where t_1 is the duration of upward section, $t_s = t_2 - t_1$, t_c is the duration of downward section. Previous research (Hu 2006) asserted that the ground motion can be truncated when the amplitude of envelope function in downward section reaches $E(t) = e^{-c(t-t_2)} = k$, in which the value of k can be defined as $1/10-1/2$. In this paper, let $k = 0.3$, and the duration of downward section t_c is calculated by

$$t_c = -\frac{\ln k}{c} \quad (2)$$

where c is attenuation coefficient of downward section.

We first statistically analyzed the value of t_1 , t_s , t_c and c for 90 magnitude-distance-site bins by calculating the amplitude envelope of acceleration recordings of every group (Amin and Ang

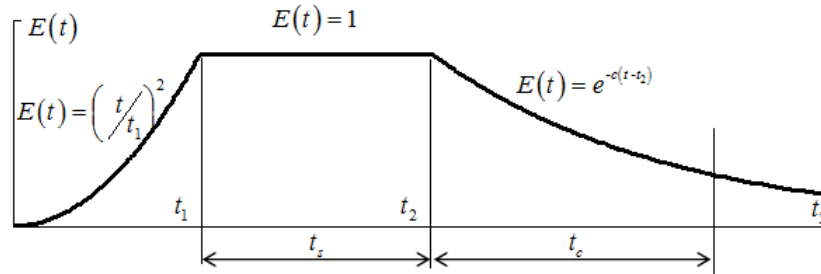


Fig. 3 Amplitude envelope function of ground motion

Table 2 The duration of accelerogram for 90 magnitude-distance-site bins (unit: s)

M	R/km	0-20			20-40			40-60			60-80			80-100			>100		
		Site	A	B	C	A	B	C	A	B	C	A	B	C	A	B	C		
	(<5.5)	25	25	25	30	30	30	30	30	30	40	40	40	40	40	45	45	45	
	[5.5,6.0)	25	25	25	30	30	30	30	30	30	40	40	50	40	40	50	70	70	70
	[6.0,6.5)	25	25	25	30	30	30	30	30	40	40	40	50	40	40	60	70	70	70
	[6.5,7.0)	25	25	25	30	30	30	30	30	40	40	40	50	40	40	40	70	70	70
	(≥7.0)	30	30	--	30	40	60	30	40	70	40	40	80	50	50	100	70	70	100

1968). Then the acceleration recordings of a given group were truncated as the same duration based on the principle, that is, $t \geq t_1 + t_s + t_c$. The uniform durations of 90 bins are shown in Table 2. Especially, the records in the bin ($M=[6.5, 7.0)$ and $R=[80-100)$ km for Site C) are relatively fewer than the rest, and durations of acceleration records are no more than 40 s. Therefore, we have to determine 40 s as the duration of this group. The result of this group is considered as an exception, and the further study will be carried out when the data are improved.

4. Simplification of non-stationarity of frequency in earthquake ground motion

4.1 Time-frequency analysis of earthquake ground-motion

The time-frequency analysis of earthquake ground-motion is to establish a two-dimensional joint distribution function with respect to time and frequency. For this purpose, some analysis techniques, such as the short time Fourier transform (STFT), continuous wavelet transform (CWT), Wigner-Ville distribution and Hilbert-Huang transform can be used to realization of the time-frequency analysis of time series. In this article, the one dimension continuous wavelet transform (CWT) is chosen to carry out analysis of ground motion because it provides flexible time-frequency windowing feature (Newland 1994). The basic idea of wavelet transform is scaling and translation, in which scaling can decompose signal in different resolution, and translation can make the decomposed signal as a window to observe what the authors concern. As a result, several wavelet functions have been developed with specified characteristic to suit for different application (Meyer 1992, Newland 1994). We choose *cmor* “ F_b ”-“ F_c ” as the wavelet base because it is a Complex-Morlet wavelet and is suitable for the analysis of earthquake ground motion. For

an acceleration time series $y(t)$, by using one-dimensional CWT with wavelet function $\varphi_{a,b}(t)$, the wavelet coefficients about time and scale can be obtained as

$$W_y(a,b) = \int_{-\infty}^{+\infty} y(t) \overline{\varphi_{a,b}(t)} dt = \frac{1}{\sqrt{|a|}} \int_{-\infty}^{+\infty} y(t) \overline{\varphi\left(\frac{t-b}{a}\right)} dt \quad (3)$$

in which, $\overline{\varphi_{a,b}(t)}$ and $\varphi_{a,b}(t)$ are pairs of conjugated wavelet base, and we have

$$\varphi_{a,b}(t) = \frac{1}{\sqrt{a}} \varphi\left(\frac{t-b}{a}\right), \quad a, b \in R, a \neq 0 \quad (4)$$

where a is scale factor, b is translation factor. Larger a corresponds to stretched wavelet, which means the wavelet function is longer in time domain, and it extracts low-frequency characteristics of signal with narrower frequency window that has higher frequency resolution. Correspondingly, smaller a corresponds to compressed wavelet, which means the wavelet function is shorter in time domain, and it extracts high-frequency characteristics of signal with wider frequency window that has lower frequency resolution.

The frequency f_a corresponding to scale factor a can be written as

$$f_a = \frac{f_c f_s}{a} \quad (5)$$

in which, f_c is the center frequency of the wavelet base $\varphi(t)$, that is $f_c=1$, and f_s is sampling frequency of acceleration record $y(t)$.

Wavelet spectrum can overcome the shortcomings of traditional spectrum that lacks of time information, and can get frequency content of signal at each time point accurately. In this paper, using one-dimensional CWT, the wavelet spectrums of 10545 records are calculated to analyze the non-stationarity of earthquake ground motion. For example, the wavelet spectrum of west-east component of recording No. 403 in NGA database is shown in Fig. 4. It can be seen that the energy distribution of earthquake in frequency and time is significantly uneven.

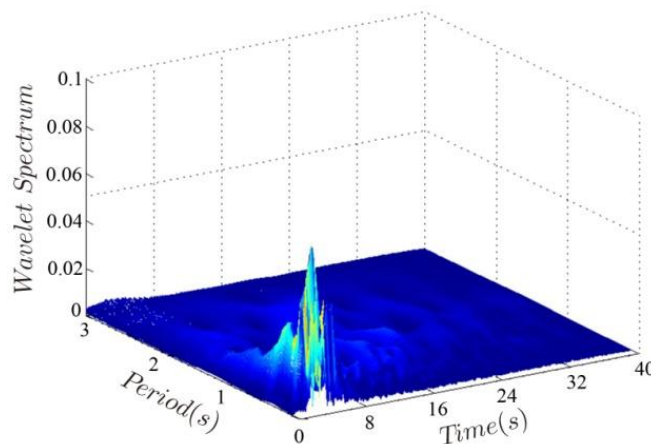


Fig. 4 The wavelet spectrum of west-east component of acceleration record No.403 in NGA database

4.2 Simplified description of non-stationarity of frequency

It is very difficult to describe the non-stationarity of frequency content by a model from the so complicated time-frequency spectrum as is shown in Fig. 4. Therefore, for the convenience of engineering application, a simplified model has to be derived to describe the variation of frequency content along with time. In this study, the frequencies (f_1, f_2, \dots, f_n) corresponding to the maximum amplitude of the wavelet spectrum at a series of sampling time (t_1, t_2, \dots, t_n) , as is shown in Fig. 5, are selected to describe the primary characteristics of time-varying frequency of earthquake ground-motion. And the frequencies (f_1, f_2, \dots, f_n) are named as the predominant frequencies.

Based on this definition, the time-varying predominant frequency of an acceleration record can be obtained, as is shown in Fig. 6, which indicates the relations between predominant frequency (f_1, f_2, \dots, f_n) and the sampling times (t_1, t_2, \dots, t_n) . Because the variation of predominant frequency changes dramatically, as is dot-line shown in Fig. 6, the authors use a moving window with fixed width $(\Delta t=0.5s)$ to scan the time-varying curve of frequencies from the beginning $t=0$ to smooth the curve. Here, suppose m is the number of frequencies in the time window, then the value of predominant frequency $f_p(t_i)$ corresponding to t_i is defined as the mean square root of frequencies within the fixed time window, that is

$$f_p(t_i) = \sqrt{\frac{f^2(t_{i-m/2}) + \dots + f^2(t_i) + \dots + f^2(t_{i+m/2})}{m}} \tag{6}$$

The smoothed curve is plotted as solid-line in Fig. 6, which can reflect the time-varying trend of predominant frequency.

After the establishment of the smoothed time-varying curve of predominant frequency of an acceleration record, we manage to analyze the variation of frequency $f_p(t)$ in a magnitude-distance-site bin. Suppose M is the number of acceleration records in a bin, for a sampling time t_i ,

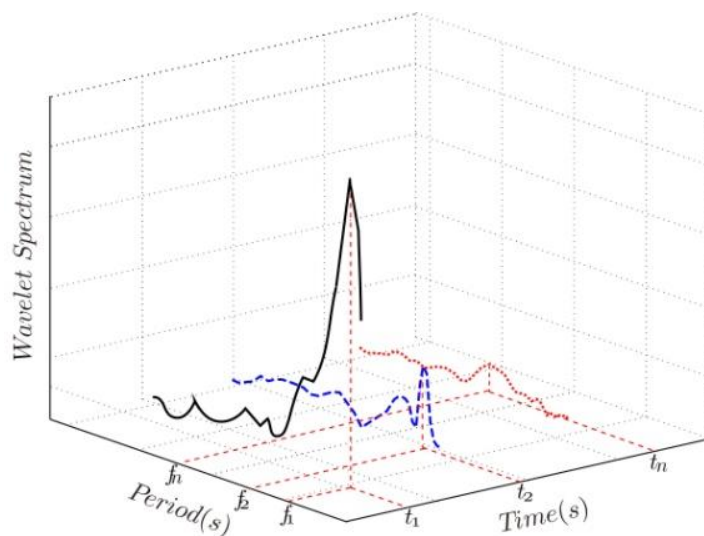


Fig. 5 Definition of predominant frequencies

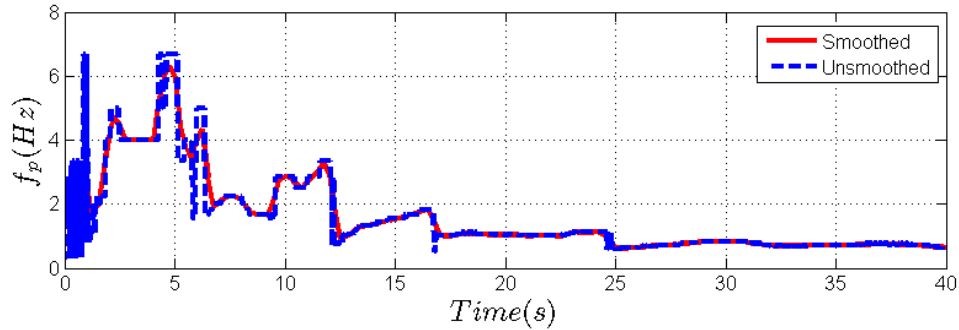


Fig. 6 Time-varying curves of the predominant frequency (west-east component of record No.403 in NGA database)

the mean square root of frequency $f_p(t_i)$ of different acceleration record, defined as $F_p(t)$, can be obtained by

$$F_p(t_i) = \sqrt{\frac{f_{p1}^2(t_i) + f_{p2}^2(t_i) + \dots + f_{pM}^2(t_i)}{M}} \quad (7)$$

in which $f_{pM}(t_i)$ represent the frequency $f_p(t_i)$ of the M -th acceleration record in this bin. The variation of $F_p(t)$ of west-east (WE) component, north-south (NS) component and vertical (UP) component in the three directions for the bin ($M=(<5.5)$ and $R=[0-20]$ km for Site A) are plotted in Fig. 7. It can be seen that the variations of $F_p(t)$ of WE and NS components have similar trends, but variation trend of UP component seems to be different with that of the horizontal components. The relevant study on the Chi-Chi earthquake showed that the characteristics of horizontal and vertical earthquake records present great discrepancies (Wang *et al.* 2002). Hence, the accelerograms in the horizontal and vertical directions are discussed separately, but the two horizontal components are no longer distinguished in this study.

After the simplification as above, the time-dependent variation of $F_p(t)$ of 178 magnitude-distance-site bins for horizontal and vertical components can be obtained. As an example, the variations of $F_p(t)$ for the two bins ($M=(<5.5)$ and $R=[80-100]$ km for Site B) and ($M=[5.5,6.0)$ and

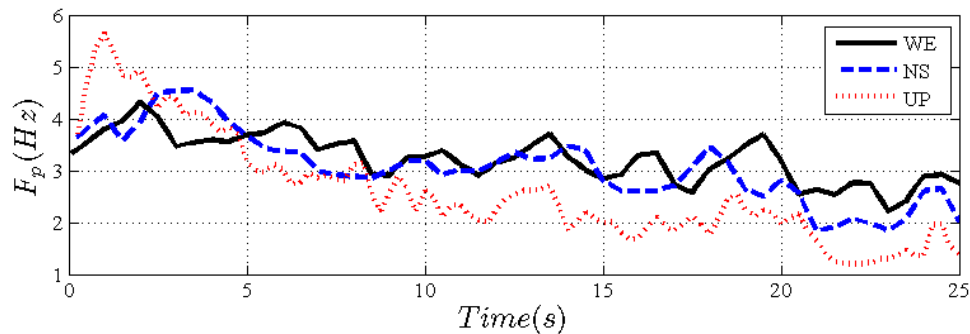


Fig. 7 Variation of predominant frequency of three components for the bin ($M=(<5.5)$ and $R=[0-20]$ km for Site A]

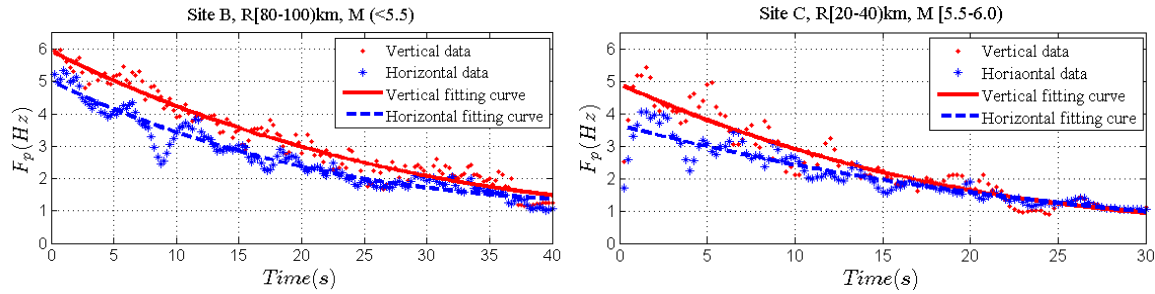


Fig. 8 Variation and fitting of predominant frequency

R=[20-40] km for Site C) are plotted in Fig. 8, in which symbol “*” and “.” respectively represent the values of $F_p(t)$ in horizontal and velocity directions.

5. Empirical model of time-varying frequency of earthquake ground motion

For the convenience of engineering practice, it is necessary to adopt a simple function model to fit the time-variation of $F_p(t)$. The statistical data as shown in Fig. 8 indicate that (1) the predominant frequency of earthquake ground motion decreases gradually along with increasing time, and (2) the decrease of the predominant frequency with increasing time in the vertical direction tends to be more obvious than that in the horizontal direction. Based on these analyses, three models, i.e., simple linear model, exponential model and exponential trigonometric model are selected to simulate the variation of $F_p(t)$. After comparing the simulation results of different model, the exponential trigonometric model, as expressed by Eq. (8), is finally selected to simulate the variation of $F_p(t)$, which can readily reflect the variation trait of the predominant frequency and is relatively simple.

$$F_p(t) = f_0 + pe^{-st} \sin(\omega t) \tag{8}$$

The parameters of Eq. (8) for 178 magnitude-distance-site-direction bins can be estimated by combining the Levenberg-Marquardt method with the universal global optimization. For Site A, the parameter $p=15$, and the other parameters are listed in the Table 3; for Site B and Site C, the parameter $p=25$, and the other parameters are listed in the Table 4 and Table 5, respectively. In which, the parameters of vertical components are underlined and the rests are horizontal parameters, and the symbol “--” means no corresponding results were obtained.

The effectiveness of the model fitting can be judged using the following indices defined as

$$r^2 = \frac{\sum(\hat{y}_i - \bar{Y})^2}{\sum(y_i - \bar{Y})^2}, \quad \sigma^2 = \frac{\sum(y_i - \hat{y}_i)^2}{n(1 - r^2)} \tag{9}$$

in which y_i is the original data, \bar{Y} represents the average value of data, \hat{y}_i is the estimated value, n denotes the number of data. r stands for the correlation coefficient, which varies from 0 to 1, and indicates the degree of coincidence of the model to the original data, that is, the closer r is to 1, the better the fitting result. As a result, σ^2 indicates the variance of the data, which represents the

degree of discreteness of the data. The values of σ^2 and r are also listed in Table 3 to Table 5. The values of σ^2 vary from 0.098 to 0.996, which indicates that the degrees of discreteness of the data are relatively small. And the r varies from 0.554 to 0.969, which indicates that the fitting parameter can be acceptable. It can be observed from Fig.8 that the model expressed by Eq. (8) gives a better fitting result of the variation of $F_p(t)$.

Table 3 Model fitting parameters for site A

M	R/km	f_0	s	ω	σ^2	r	R/km	f_0	s	ω	σ^2	r	
<5.5	0~20	<u>5.563</u>	<u>0.045</u>	<u>-0.034</u>	<u>0.401</u>	<u>0.932</u>	20~40	<u>5.941</u>	<u>0.061</u>	<u>-0.035</u>	<u>0.678</u>	<u>0.705</u>	
		4.385	0.014	-0.007	0.349	0.836		5.745	0.075	-0.016	0.340	0.600	
	40~60	<u>5.536</u>	<u>-0.070</u>	<u>-0.001</u>	<u>0.837</u>	<u>0.844</u>	60~80	<u>5.474</u>	<u>-0.013</u>	<u>-0.004</u>	<u>0.857</u>	<u>0.886</u>	
		3.787	0.013	-0.004	0.484	0.571		6.139	-0.021	-0.002	0.558	0.870	
	80~100	<u>5.229</u>	<u>0.012</u>	<u>-0.011</u>	<u>0.559</u>	<u>0.897</u>	≥ 100	<u>4.346</u>	<u>0.019</u>	<u>-0.013</u>	<u>0.511</u>	<u>0.884</u>	
		5.488	0.002	-0.006	0.408	0.924		3.469	0.007	-0.003	0.466	0.713	
	[5.5,6.0)	0~20	<u>5.110</u>	<u>0.053</u>	<u>-0.033</u>	<u>0.394</u>	<u>0.906</u>	20~40	<u>5.045</u>	<u>0.030</u>	<u>-0.023</u>	<u>0.565</u>	<u>0.892</u>
			3.556	0.052	-0.015	0.261	0.844		5.708	0.060	-0.032	0.497	0.779
40~60		<u>4.634</u>	<u>0.020</u>	<u>-0.015</u>	<u>0.407</u>	<u>0.928</u>	60~80	<u>5.363</u>	<u>0.023</u>	<u>-0.019</u>	<u>0.448</u>	<u>0.934</u>	
		5.226	0.022	-0.017	0.374	0.945		3.790	0.013	-0.008	0.298	0.931	
80~100		<u>4.854</u>	<u>0.020</u>	<u>-0.013</u>	<u>0.496</u>	<u>0.894</u>	≥ 100	<u>3.279</u>	<u>0.009</u>	<u>-0.004</u>	<u>0.407</u>	<u>0.866</u>	
		5.424	0.014	-0.014	0.394	0.954		3.666	0.015	-0.006	0.329	0.889	
[6.0,6.5)		0~20	<u>4.101</u>	<u>0.051</u>	<u>-0.029</u>	<u>0.502</u>	<u>0.849</u>	20~40	<u>4.472</u>	<u>0.029</u>	<u>-0.022</u>	<u>0.356</u>	<u>0.950</u>
			2.909	0.042	-0.010	0.495	0.581		3.440	0.007	-0.008	0.232	0.961
	40~60	<u>4.894</u>	<u>0.028</u>	<u>-0.018</u>	<u>0.386</u>	<u>0.937</u>	60~80	<u>5.339</u>	<u>0.021</u>	<u>-0.015</u>	<u>0.307</u>	<u>0.959</u>	
		4.856	0.020	-0.013	0.292	0.951		4.971	0.020	-0.012	0.258	0.962	
	80~100	<u>5.485</u>	<u>0.017</u>	<u>-0.015</u>	<u>0.445</u>	<u>0.941</u>	≥ 100	<u>3.974</u>	<u>0.010</u>	<u>-0.007</u>	<u>0.327</u>	<u>0.947</u>	
		5.592	0.020	-0.016	0.288	0.969		4.094	0.012	-0.007	0.327	0.937	
	[6.5,7.0)	0~20	<u>5.596</u>	<u>-0.014</u>	<u>-0.009</u>	<u>0.551</u>	<u>0.938</u>	20~40	<u>3.721</u>	<u>0.029</u>	<u>-0.012</u>	<u>0.381</u>	<u>0.848</u>
			2.773	-0.044	-0.001	0.255	0.805		3.443	0.030	-0.009	0.220	0.903
40~60		<u>4.790</u>	<u>0.022</u>	<u>-0.018</u>	<u>0.450</u>	<u>0.934</u>	60~80	<u>5.097</u>	<u>0.027</u>	<u>-0.025</u>	<u>0.342</u>	<u>0.963</u>	
		3.530	-0.024	-0.003	0.316	0.942		4.629	0.023	-0.017	0.324	0.959	
80~100		<u>2.604</u>	<u>0.005</u>	<u>-0.004</u>	<u>0.345</u>	<u>0.883</u>	≥ 100	<u>2.482</u>	<u>0.019</u>	<u>-0.006</u>	<u>0.287</u>	<u>0.843</u>	
		2.234	0.009	-0.003	0.235	0.850		3.254	0.013	-0.006	0.345	0.886	
≥ 7.0		0~20	<u>3.354</u>	<u>-0.054</u>	<u>-0.001</u>	<u>0.586</u>	<u>0.736</u>	20~40	<u>3.000</u>	<u>0.022</u>	<u>-0.009</u>	<u>0.413</u>	<u>0.812</u>
			2.501	0.050	-0.001	0.412	0.744		2.505	0.027	-0.005	0.172	0.868
	40~60	<u>4.163</u>	<u>0.044</u>	<u>-0.021</u>	<u>0.608</u>	<u>0.743</u>	60~80	<u>4.176</u>	<u>-0.002</u>	<u>-0.006</u>	<u>0.387</u>	<u>0.941</u>	
		4.172	0.058	-0.014	0.471	0.554		4.113	0.016	-0.009	0.304	0.934	
	80~100	<u>3.410</u>	<u>-0.001</u>	<u>-0.004</u>	<u>0.425</u>	<u>0.897</u>	≥ 100	<u>2.733</u>	<u>0.004</u>	<u>-0.003</u>	<u>0.241</u>	<u>0.941</u>	
		3.243	0.011	-0.004	0.243	0.917		3.250	0.006	-0.004	0.248	0.952	

Note: the model parameters of the vertical components are underlined and the rests are the horizontal parameters

Table 4 Model fitting parameters for site B

M	R/km	f_0	s	ω	σ^2	r	R/km	f_0	s	ω	σ^2	r	
<5.5	0~20	<u>5.555</u>	<u>0.038</u>	<u>-0.018</u>	<u>0.235</u>	<u>0.980</u>	20~40	<u>5.429</u>	<u>0.030</u>	<u>-0.012</u>	<u>0.229</u>	<u>0.973</u>	
		4.594	0.030	-0.010	0.229	0.974		4.145	0.037	-0.008	0.185	0.945	
	40~60	<u>5.331</u>	<u>0.012</u>	<u>-0.006</u>	<u>0.381</u>	<u>0.914</u>	60~80	<u>6.051</u>	<u>0.023</u>	<u>-0.010</u>	<u>0.296</u>	<u>0.961</u>	
		4.658	0.024	-0.008	0.275	0.945		4.955	0.017	-0.005	0.175	0.971	
	80~100	<u>5.942</u>	<u>0.014</u>	<u>-0.008</u>	<u>0.285</u>	<u>0.975</u>	≥ 100	<u>5.197</u>	<u>0.009</u>	<u>-0.005</u>	<u>0.446</u>	<u>0.922</u>	
		5.016	0.018	-0.008	0.277	0.966		4.268	0.011	-0.004	0.272	0.949	
	[5.5,6.0)	0~20	<u>5.819</u>	<u>0.047</u>	<u>-0.024</u>	<u>0.303</u>	<u>0.969</u>	20~40	<u>6.250</u>	<u>0.037</u>	<u>-0.020</u>	<u>0.317</u>	<u>0.971</u>
			3.570	0.041	-0.010	0.165	0.967		4.443	0.039	-0.012	0.167	0.978
40~60		<u>5.564</u>	<u>0.029</u>	<u>-0.014</u>	<u>0.308</u>	<u>0.968</u>	60~80	<u>4.874</u>	<u>0.022</u>	<u>-0.009</u>	<u>0.326</u>	<u>0.955</u>	
		4.715	0.025	-0.010	0.258	0.965		3.996	0.018	-0.006	0.242	0.958	
80~100		<u>3.911</u>	<u>0.010</u>	<u>-0.004</u>	<u>0.262</u>	<u>0.941</u>	≥ 100	<u>3.513</u>	<u>0.013</u>	<u>-0.004</u>	<u>0.219</u>	<u>0.965</u>	
		3.631	0.015	-0.004	0.213	0.943		3.089	0.011	-0.003	0.202	0.963	
[6.0,6.5)		0~20	<u>4.804</u>	<u>0.023</u>	<u>-0.011</u>	<u>0.499</u>	<u>0.905</u>	20~40	<u>5.086</u>	<u>0.026</u>	<u>-0.012</u>	<u>0.334</u>	<u>0.960</u>
			3.651	0.035	-0.008	0.295	0.891		3.788	0.025	-0.007	0.201	0.962
	40~60	<u>4.750</u>	<u>0.019</u>	<u>-0.009</u>	<u>0.268</u>	<u>0.973</u>	60~80	<u>4.951</u>	<u>0.020</u>	<u>-0.009</u>	<u>0.258</u>	<u>0.974</u>	
		4.061	0.023	-0.008	0.232	0.962		4.515	0.020	-0.008	0.223	0.974	
	80~100	<u>4.487</u>	<u>0.018</u>	<u>-0.007</u>	<u>0.242</u>	<u>0.969</u>	≥ 100	<u>3.734</u>	<u>0.012</u>	<u>-0.004</u>	<u>0.197</u>	<u>0.976</u>	
		4.321	0.020	-0.007	0.171	0.982		3.323	0.014	-0.004	0.184	0.9722	
	[6.5,7.0)	0~20	<u>4.799</u>	<u>0.011</u>	<u>-0.007</u>	<u>0.453</u>	<u>0.900</u>	20~40	<u>4.765</u>	<u>0.021</u>	<u>-0.010</u>	<u>0.284</u>	<u>0.969</u>
			2.631	0.005	-0.002	0.209	0.883		2.885	0.017	-0.004	0.184	0.939
40~60		<u>4.856</u>	<u>0.007</u>	<u>-0.006</u>	<u>0.315</u>	<u>0.962</u>	60~80	<u>4.772</u>	<u>0.020</u>	<u>-0.009</u>	<u>0.339</u>	<u>0.959</u>	
		3.392	0.008	-0.004	0.219	0.951		3.346	0.016	-0.005	0.120	0.988	
80~100		<u>3.294</u>	<u>0.006</u>	<u>-0.003</u>	<u>0.231</u>	<u>0.952</u>	≥ 100	<u>2.927</u>	<u>0.008</u>	<u>-0.002</u>	<u>0.236</u>	<u>0.935</u>	
		3.178	0.007	-0.003	0.163	0.971		2.386	0.014	-0.002	0.140	0.946	
≥ 7.0		0~20	<u>4.678</u>	<u>0.026</u>	<u>-0.010</u>	<u>0.706</u>	<u>0.801</u>	20~40	<u>3.983</u>	<u>0.028</u>	<u>-0.009</u>	<u>0.452</u>	<u>0.871</u>
			2.683	0.048	-0.006	0.421	0.550		3.197	0.029	-0.007	0.242	0.925
	40~60	<u>3.425</u>	<u>0.024</u>	<u>-0.007</u>	<u>0.282</u>	<u>0.938</u>	60~80	<u>4.067</u>	<u>0.010</u>	<u>-0.005</u>	<u>0.289</u>	<u>0.958</u>	
		2.671	0.028	-0.005	0.178	0.927		3.821	0.021	-0.006	0.193	0.967	
	80~100	<u>4.056</u>	<u>0.004</u>	<u>-0.003</u>	<u>0.327</u>	<u>0.946</u>	≥ 100	<u>3.079</u>	<u>0.008</u>	<u>-0.002</u>	<u>0.206</u>	<u>0.959</u>	
		3.727	0.017	-0.005	0.201	0.966		2.708	0.011	-0.002	0.098	0.983	

Note: the model parameters of the vertical components are underlined and the rests are the horizontal parameters

Now we defined variance coefficient

$$H_{cov} = \sigma[F_p(t)] / \mu[F_p(t)] \tag{10}$$

to measure the degree of non-stationary of frequency content in earthquake ground motion, and the bigger H_{cov} is, the more obvious non-stationarity of frequency content in ground motion will be

Table 5 Model fitting parameters for site C

M	R/km	f_0	s	ω	σ^2	r	R/km	f_0	s	ω	σ^2	r	
<5.5	0~20	<u>5.480</u>	<u>0.017</u>	<u>-0.011</u>	<u>0.357</u>	<u>0.962</u>	20~40	<u>6.198</u>	<u>0.018</u>	<u>-0.011</u>	<u>0.572</u>	<u>0.922</u>	
		3.351	0.002	-0.004	0.261	0.931		4.194	0.032	-0.010	0.282	0.941	
	40~60	<u>5.097</u>	<u>0.004</u>	<u>-0.006</u>	<u>0.509</u>	<u>0.910</u>	60~80	<u>6.393</u>	<u>0.037</u>	<u>-0.022</u>	<u>0.692</u>	<u>0.885</u>	
		4.534	0.025	-0.009	0.443	0.894		5.242	0.027	-0.012	0.604	0.884	
	80~100	<u>5.762</u>	<u>0.028</u>	<u>-0.015</u>	<u>0.561</u>	<u>0.912</u>	≥ 100	<u>4.207</u>	<u>0.009</u>	<u>-0.004</u>	<u>0.380</u>	<u>0.917</u>	
		3.277	0.027	-0.006	0.253	0.915		4.319	0.006	-0.004	0.264	0.966	
	[5.5,6.0)	0~20	<u>5.923</u>	<u>0.011</u>	<u>-0.010</u>	<u>0.607</u>	<u>0.915</u>	20~40	<u>4.908</u>	<u>0.021</u>	<u>-0.010</u>	<u>0.413</u>	<u>0.939</u>
			3.158	0.013	-0.005	0.327	0.886		3.631	0.018	-0.006	0.313	0.924
40~60		<u>5.392</u>	<u>0.017</u>	<u>-0.010</u>	<u>0.526</u>	<u>0.922</u>	60~80	<u>5.864</u>	<u>0.007</u>	<u>-0.006</u>	<u>0.757</u>	<u>0.906</u>	
		5.055	0.024	-0.011	0.380	0.944		4.690	0.012	-0.006	0.658	0.870	
80~100		<u>4.738</u>	<u>0.005</u>	<u>-0.004</u>	<u>0.584</u>	<u>0.897</u>	≥ 100	<u>3.686</u>	<u>0.008</u>	<u>-0.003</u>	<u>0.301</u>	<u>0.948</u>	
		4.150	0.003	-0.003	0.505	0.895		3.296	0.011	-0.003	0.215	0.962	
[6.0,6.5)		0~20	<u>6.505</u>	<u>0.054</u>	<u>-0.034</u>	<u>0.996</u>	<u>0.820</u>	20~40	<u>5.256</u>	<u>0.034</u>	<u>-0.018</u>	<u>0.429</u>	<u>0.952</u>
			5.742	0.059	-0.032	0.743	0.849		4.935	0.033	-0.016	0.353	0.962
	40~60	<u>4.210</u>	<u>0.020</u>	<u>-0.008</u>	<u>0.325</u>	<u>0.957</u>	60~80	<u>4.096</u>	<u>0.007</u>	<u>-0.004</u>	<u>0.455</u>	<u>0.921</u>	
		4.165	0.029	-0.011	0.286	0.961		4.210	0.015	-0.006	0.411	0.939	
	80~100	<u>3.244</u>	<u>0.003</u>	<u>-0.002</u>	<u>0.391</u>	<u>0.897</u>	≥ 100	<u>3.623</u>	<u>0.012</u>	<u>-0.004</u>	<u>0.236</u>	<u>0.966</u>	
		3.796	0.015	-0.005	0.388	0.929		3.174	0.018	-0.005	0.189	0.967	
	[6.5,7.0)	0~20	<u>6.488</u>	<u>0.003</u>	<u>-0.009</u>	<u>0.640</u>	<u>0.925</u>	20~40	<u>5.278</u>	<u>0.019</u>	<u>-0.011</u>	<u>0.488</u>	<u>0.947</u>
			1.714	0.001	-0.001	0.274	0.526		2.615	0.014	-0.004	0.329	0.874
40~60		<u>5.235</u>	<u>0.026</u>	<u>-0.013</u>	<u>0.359</u>	<u>0.964</u>	60~80	<u>4.567</u>	<u>0.020</u>	<u>-0.009</u>	<u>0.487</u>	<u>0.919</u>	
		2.621	0.018	-0.004	0.132	0.976		2.640	0.010	-0.003	0.205	0.955	
80~100		<u>4.252</u>	<u>0.032</u>	<u>-0.012</u>	<u>0.491</u>	<u>0.872</u>	≥ 100	<u>4.143</u>	<u>0.023</u>	<u>-0.009</u>	<u>0.397</u>	<u>0.914</u>	
		2.461	0.025	-0.005	0.197	0.937		1.409	0.014	-0.001	0.117	0.852	
≥ 7.0		0~20	--	--	--	--	--	20~40	<u>5.290</u>	<u>0.019</u>	<u>-0.010</u>	<u>0.658</u>	<u>0.907</u>
			--	--	--	--	--		4.030	0.021	-0.008	0.268	0.960
	40~60	<u>5.104</u>	<u>0.016</u>	<u>-0.008</u>	<u>0.459</u>	<u>0.945</u>	60~80	<u>4.250</u>	<u>0.015</u>	<u>-0.006</u>	<u>0.471</u>	<u>0.914</u>	
		4.630	0.018	-0.008	0.278	0.969		3.620	0.018	-0.006	0.334	0.931	
	80~100	<u>3.055</u>	<u>0.011</u>	<u>-0.003</u>	<u>0.254</u>	<u>0.945</u>	≥ 100	<u>2.653</u>	<u>0.012</u>	<u>-0.003</u>	<u>0.201</u>	<u>0.951</u>	
		3.650	0.012	-0.004	0.201	0.973		2.437	0.014	-0.003	0.115	0.976	

Note: the model parameters of the vertical components are underlined and the rests are the horizontal parameters. And the symbol "--" means that no corresponding results have been obtained

(Yang and Wang 2012). In which, $\sigma[F_p(t)]$ and $\mu[F_p(t)]$ respectively represent the standard deviation and mean value of $F_p(t)$.

The variations of H_{cov} of 178 magnitude-distance-site-direction bins are plotted in Fig. 9, it can be seen that: (1) For the Site A, the value of H_{cov} of vertical component is generally more than that of horizontal components. Along with the site condition gets tender gradually, the difference between vertical and horizontal components becomes smaller, which indicates that site condition

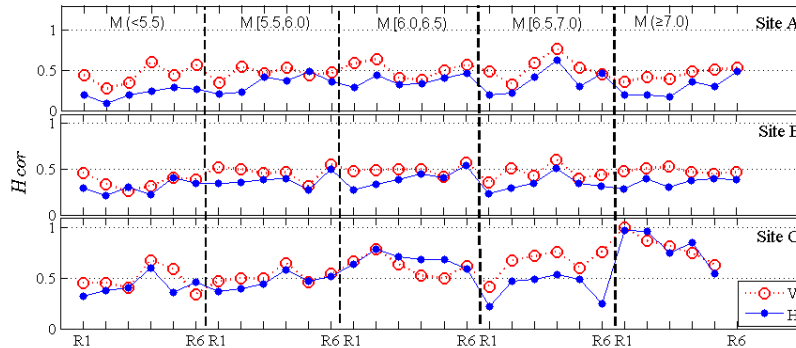


Fig. 9 The variable coefficient for magnitude-distance-site-direction bins

influences the non-stationarity of frequency content at different directions. (2) Comparatively, values of H_{cov} for Site C will be bigger than the values for Site A and B. It means that along with the site condition becomes softer, the non-stationarity of frequency content in ground motion becomes more obvious. In summary, under the condition of large magnitude, the non-stationarity of frequency content of ground motion in near field and under softer site condition is more obvious.

6. Practical frequency-dependent amplitude envelope function

Currently, the most commonly used random model to generate an artificial seismic wave can be written as

$$y(t) = E(t)x(t) \tag{11}$$

where $E(t)$ is a deterministic absolute amplitude envelope function with maximum value of 1, and $x(t)$ is a stationary random process with a power spectral density function $S(\omega)$. However, Eq. (11) failed to characterize the time-varying nature of frequencies in earthquake ground motion. Therefore, the evolutionary random process model was proposed to reflect the non-stationary frequency content in the artificial simulation of ground-motion (Nigam 1983), that is

$$y(t) = \int_{-\infty}^{\infty} B(t, \omega) e^{i\omega t} dF(\omega) \tag{12}$$

where $i = \sqrt{-1}$, and $B(t, \omega)$ is a deterministic time-frequency modulating function. Consequently, it represents an absolute amplitude envelope of a seismic process. $dF(\omega)$ is a zero-mean, mutually independent, orthogonal increment process with

$$E[dF(\omega)] = 0 \tag{13}$$

$$E[dF^*(\omega_1)dF(\omega_2)] = \delta(\omega_1 - \omega_2)S(\omega_1)d\omega_1d\omega_2 \tag{14}$$

in which $E[.]$ denotes the ensemble average, $\delta(\cdot)$ is the Dirac delta function, “*” stands for the

complex conjugate, and $S(\omega)$ is the power spectral density function of $dF(\omega)$.

In earthquake engineering applications, the time-frequency modulating function only make sense when it is real and non-negative, that is

$$B(t, \omega) \in R, B(t, \omega) \geq 0$$

Suppose, for a given frequency ω_i , $B(t, \omega)$ is normalized as

$$\max [B(t, \omega_i)] = 1 \tag{15}$$

Then $B(t, \omega_i)$ only determines the shape of intensity envelop (for different frequency) of earthquake ground motion, while the amplitude for ω_i of earthquake ground motion is controlled by $S(\omega_i)$.

Based on Eq. (12), the following trigonometric method is employed to generate artificial seismic wave

$$y(t) = \sum_{i=1}^n B(t, \omega_i) 2\sqrt{S(\omega_i)\Delta\omega} \cos(\omega_i t + \varphi_i) \tag{16}$$

in which $\Delta\omega$ is the frequency increment, ω_i is the discrete frequency, and φ_i is the random phase with uniform distribution from 0 to 2π .

Obviously, if the joint time-frequency distribution of $B(t, \omega)$ can be estimated reasonably based on engineering requirement, the solution of Eq. (16) is not difficult. However, owing to the complexity and uncertainty of earthquake ground motion, some joint descriptions of the time-frequency model include many model parameters, which are difficult to be directly used in engineering practice. Therefore, we managed to develop a practical frequency-dependent amplitude envelope function based on the time-variation of predominant frequency described by Eq. (8) derived in this paper.

For a series of sampling time t_i , the frequency-dependent variation of spectrum can be described by a single parameter function, that is

$$L(f, t_i) = \frac{f}{F_p(t_i)} e^{-\frac{f-F_p(t_i)}{F_p(t_i)}} \tag{17}$$

where f is frequency, $F_p(t_i)$ represents the predominant frequency corresponding to sampling time t_i , which can be calculated by Eq. (8).

If using $E(t)$ to describe the amplitude variation of seismic ground motion, the joint distribution of time-frequency of earthquake ground motion can be defined as

$$WB(t, f) = E^2(t)L(f, t) \tag{18}$$

Then the frequency-dependent envelope function of ground motion $B(t, f_i)$ corresponding to f_i can be obtained by normalizing the $WB(t, f)$, that is

$$B(t, f_i) = WB(t, f_i) / \max [WB(t, f_i)] \quad i=1, 2, \dots \tag{19}$$

where f_i is the discrete frequency.

Now an example of simulating artificial earthquake ground motion based on Eq. (16) and Eq. (19) will be given. Select double exponential function (Shinozuka and Sato 1967, Iyengar and Iyengar 1969) to describe the intensity variation of ground motion, i.e.

$$E(t) = I_0 (e^{-\alpha t} - e^{-\beta t}) \tag{20}$$

and let $\alpha=0.08595$, $\beta=0.3$, $I_0=2.3152$, we can obtain the amplitude envelope function. And suppose time-variation of frequency is modeled as

$$F_p(t) = 5.097 + 15_1 e^{-0.027t} \sin(-0.025t) \tag{21}$$

which is determined based on the parameters corresponding the bin ($M[6.5,7.0]$ and $R[60-80]$ for Site A), as is shown in Table 3. Then the envelope functions $B(t, f_i)$ of ground motion corresponding to f_i can be obtained. The variations of $B(t, f_i)$ at frequencies 0.8 Hz, 5.0 Hz, 10 Hz and 15 Hz are shown in Fig. 10, in which the times corresponding to peak values of different frequencies are respectively 7.39s, 5.20s, 4.10s and 3.45s. Obviously, for different frequencies f_i , seismic ground motion amplitudes have rather different patterns. In all four cases, as frequency increases, the low-frequency contents become more and more prominent, implying that the

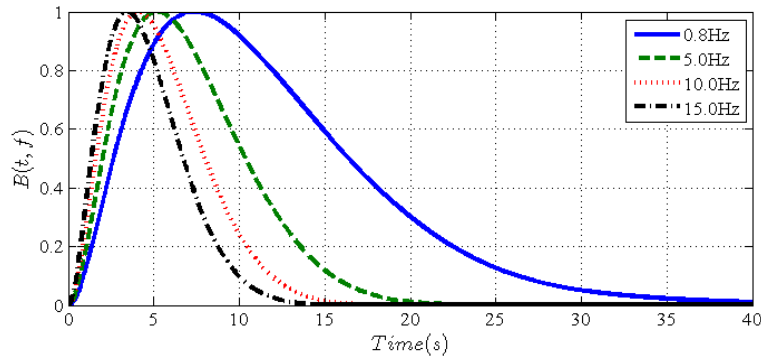


Fig. 10 Variation of frequency-dependent amplitude envelope function at different frequency

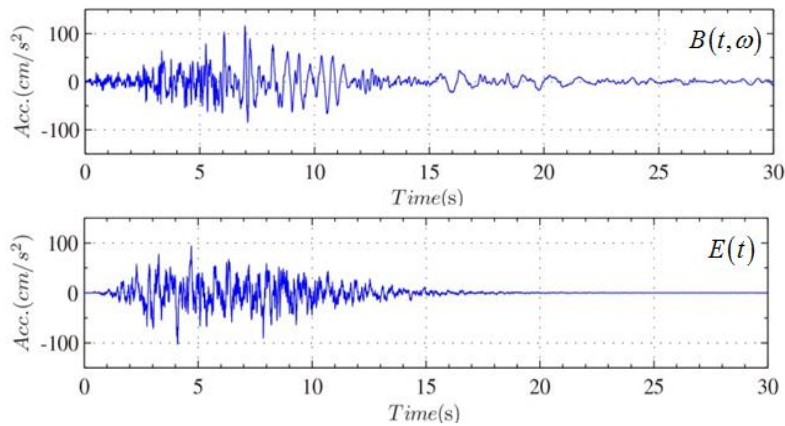


Fig. 11 Acceleration time histories simulated by different envelope functions

frequency-dependent modulating function $B(t, f_i)$ emphasizes the effect of low-frequency components in later seismic actions. Suppose the power spectral density function $S(\omega)$ is modeled as

$$S(\omega) = \frac{\omega^6}{\omega^6 + \omega_c^6} \frac{\omega_g^4 + 4\xi_g^2 \omega_g^2 \omega^2}{(\omega_g^2 - \omega^2)^2 + 4\xi_g^2 \omega_g^2 \omega^2} S_0 \quad (22)$$

where $\zeta_g=0.72$, $\omega_g=15.71$ rad/s, $\omega_c=3.11$ rad/s, $S_0=18.5$ cm/s². We can get the artificial acceleration time history based on Eq. (16), in which the frequency-dependent envelope function described by Eq. (19). In order to compare the effect the envelope function, the function $B(t, f_i)$ of Eq. (16) is replaced by $E(t)$, and a new artificial acceleration time series can be obtained. The two time histories based on different amplitude envelope functions are shown in Fig. 11. It is obvious that the artificial wave based on frequency-dependent envelope function $B(t, f_i)$ can reflect preferably the non-stationarity of the frequency content in earthquake ground motions.

In practice, any satisfying model should have as few parameters as possible, and has a form, which facilitates the engineering applications. The frequency-dependent envelope function of ground motion $B(t, f)$ derived by Eq. (19) has clear statistical parameters that have been listed in tables for different magnitude, distance, site conditions and direction requirements. It can also consider the non-stationary of frequency content in ground motion, especially emphasize the effect of low-frequency components in later seismic action. Therefore, this model is valuable in simulation of ground motion to reflect the non-stationary of earthquake acceleration.

7. Conclusions

In this study, we selected 10545 acceleration recordings from the NGA database and binned by magnitude, distance, site condition and direction, and the non-stationarity of frequency content in earthquake ground motion was analyzed by using the one-dimension continuous wavelet transform. The conclusions obtained in this study are as follows:

(1) The frequencies corresponding to the maximum values of the wavelet spectrum at a series of sampling time, named as predominant frequency, are selected to analyze the primary variations of the frequency content in earthquake ground motion. Consequently, the time-variations of the predominant frequencies for 178 magnitude-distance-site-direction bins are obtained by calculating the mean square root of predominant frequencies within a bin. The results illustrate that the time-varying predominant frequency can preferably reflect the non-stationarity of the frequency content in earthquake ground motions.

(2) The exponential trigonometric model is selected to fit the data of time-varying frequency, which describes the predominant frequency of motion as a function of time with model parameters given in tables for different magnitude, distance, site conditions and direction requirements. The model can be used to research the time-variation of frequencies content, and can also be used as a reference for synthesizing artificial acceleration time-series so as to analyze structural nonlinear responses.

(3) Finally, a frequency-dependent amplitude envelope function is developed based on the time-varying frequency derived in this study, which can consider the non-stationary of frequency content in ground motion, especially emphasize the effect of low-frequency components in later seismic action. As a result, this model has clear statistical parameters according to the recording

direction, magnitude, distance and site condition. In addition, it can be used in simulation of ground motion to reflect the non-stationary of earthquake acceleration.

Acknowledgments

The research described in this paper was financially supported by the Natural Science Foundation of China (No. 51108429 and No. 51478440) and National Key Technology R&D Program (2012BAK15B01). The used strong-motion data were chosen from PEER.

References

- Amin, M. and Ang, A.H.S. (1968), "Nonstationary stochastic models of earthquake", *J. Eng. Mech.*, ASCE, **94**, 559-583.
- Bozorgnia, Y. and Bertero, V.V. (2004), *Earthquake Engineering: from Engineering Seismology to Performance-based Engineering*, CRC Press, Boca Raton, Fla.
- Cakir, T. (2013), "Evaluation of the effect of earthquake frequency content on seismic behavior of cantilever retaining wall including soil-structure interaction", *Soil Dyn. Earthq. Eng.*, **45**, 96-111.
- Chiou, B., Darragh, R., Gregor, N. and Silva, W. (2008), "NGA project strong-motion database", *Earthq. Spectra*, **24**(1), 23-44.
- Conte, J.P. and Peng, B.F. (1997), "Fully non-stationary analytical earthquake ground-motion model", *J. Eng. Mech.*, ASCE, **123**(1), 15-24.
- Deodatis, G. and Shinozuka, M. (1988), "Auto-regressive model for nonstationary stochastic process", *J. Eng. Mech.*, ASCE, **114**(11), 1995-2012.
- Gabor, D. (1946), "Theory of communication", *J. Inst. Electr. Eng.*, **93**, 429-457.
- Housner, G.W. and Jennings, P.C. (1964), "Generation of artificial earthquake", *J. Eng. Mech.*, **90**(EM1), 113-150.
- Hu, Y.X. (2006), *Earthquake Engineering (the second edition)*, Earthquake Publishing House, Beijing.
- Jin, X.L., Huang, Z.L. and Leung, A.Y.T. (2012), "Non-stationary seismic responses of structure with nonlinear stiffness subject to modulated Kanai-Tajimi excitation", *Earthq. Eng. Struct. Dyn.*, **41**(2), 197-210.
- Lü, H.S. and Zhao, F.X. (2007), "Site coefficients suitable to China site category", *Acta Seismologica Sinica*, **20**, 71-79.
- Meyer, Y. (1992), *Wavelets and Operators*, Cambridge University Press, New York.
- Nakayama, T., Fujiwara, H., Komatsu, S. and Sumida, N. (1994), "Nonstationary response and reliability of linear systems under seismic loadings", *Struct. Saf. Reliab.*, Rotterdam: Balkema, 2179-2186.
- Newland, D.E. (1994), "Wavelet analysis of vibration, Part 2: Wavelet maps", *J. Vib. Acoustics*, **116**(4), 417-425.
- Nimtaj, A. and Bagheripour, M.H. (2013), "Non-linear seismic response analysis of the layered soil deposit using hybrid frequency-time domain (HFTD) approach", *Euro. J. Envir. Civ. Eng.*, **17**(10), 1039-1056.
- O'Neill, J.C., Flandrin, P. and Williams, W.J. (1999), "On the existence of discrete Wigner distributions", *Sig. Proc. Lett.*, IEEE, **6**(12), 304-306.
- Papadimitriou, K. (1990), "Stochastic characterization of strong ground motion and application to structural response", *Report No. EERL 90-03, Earthquake Engineering Research Laboratory*, California Institute of Technology, Pasadena, CA.
- Rezaeian, S. and Der Kiureghian, A. (2008), "A stochastic ground motion model with separable temporal and spectral nonstationarities", *Earthq. Eng. Struct. Dyn.*, **37**(13), 1565-1584.
- Rioul, O. and Vetterli, M. (1991), "Wavelets and signal processing", *Sig. Proc.*, IEEE, **8**(4), 14-38.

- Wang, G.Q., Zhou, X.Y., Zhang, P. and Igel, H. (2002), "Characteristics of amplitude and duration for near fault strong ground motion from the 1999 Chi-Chi, Taiwan earthquake", *Soil Dyn. Earthq. Eng.*, **22**(1), 73-96.
- Wang, J.J., Fan, L.C., Qian, S. and Zhou, J. (2002), "Simulations of non-stationary frequency content and its importance to seismic assessment of structures", *Earthq. Eng. Struct. Dyn.*, **31**(4), 993-1005.
- Yang, D.X. and Wang, W. (2012), "Nonlocal period parameters of frequency content characterization of near-fault ground motions", *Earthq. Eng. Struct. Dyn.*, **41**(13), 1793-1811.
- Yeh, C.H. and Wen, Y.K. (1990), "Modeling of non-stationary ground motion and analysis of inelastic structural response", *Struct. Saf.*, **8**(1-4), 281-298.
- Zhou, X.Y. and Yu, R.F. (2008), "Mode Superposition method of non-stationary seismic response for non-classically damped system", *J. Earthq. Eng.*, **12**(3), 473-516.